Textile Science & Research Journal
ISSN: 3059-846X, Volume – 2, Issue – 1, 2026
DOI: https://doi.org/10.63456/tsrj-2-1-35

ENGINEERING ALL-TEXTILE PIEZORESISTIVE SENSORS BY PROGRAMMING STITCHING GEOMETRY

ZEWEN ZHAO[1], XINRU LI[1], XUZHONG SU[1], FENGXIN SUN*[1,2]

[1]College of Textile Science and Engineering, Jiangnan University, Wuxi 214122, China

[2]Laboratory of Soft Fibrous Materials and Physics, Center for Textile-X, Jiangnan University, Wuxi 214122, China

Fengxin Sun: fxsun@jiangnan.edu.cn

Corresponding Author: FENGXIN SUN

ABSTRACT

Textile-based piezoresistive sensors are highly desirable for wearable health monitoring, soft robotics, and human-machine interfaces due to their inherent conformability, breathability, and skin friendliness. However, the complex fabrication processes and limited scalability of current textile sensors hinder their practical use, and customizing such sensors remains challenging owing to their intricate geometry-electromechanical coupling and demanding requirements for manufacturing. Herein, we report a simple sewing-based strategy that uses stitch architecture and sewing geometry as active design parameters to tailor the electromechanical response of textile piezoresistive sensors. Systematic tuning of stitch-related geometric variables reveals the structure-property relationships that govern electrical resistance evolution, enabling programmable sensitivity, dynamic behavior, and operating pressure range through a textile-compatible, scalable fabrication process. Guided by this understanding, we fabricated an optimized stitched sensor with high sensitivity (3.4 % kPa-1), fast response (40ms) and recovery (20ms), low hysteresis (< 3%), and stable cycling performance. The programming stitch strategy offers a low-cost and manufacturing-ready route toward textile sensors with tunable electromechanical characteristics, potentially expanding their use in wearable systems and soft robotic applications.

KEYWORDS: Textile sensors, stitching design, encoded sewing, wearable electronics

1. INTRODUCTION

Flexible piezoresistive sensors have been widely used in wearable electronics, human-machine interfaces, and soft robotic systems owing to their lightweight nature, mechanical compliance, and the ability to resolve subtle pressure and deformation cues.[1, 2] Among various transduction mechanisms, piezoresistive sensors with their stable signal readout, low power consumption and good compatibility with diverse conductive materials and fabric architectures, are intensively used in textile sensing platforms.[3-5]

Various fabrication strategies have been explored to impart piezoresistive functionality to textiles,[6] in which knitted piezoresistive sensors leverage the looped geometry of weft- and warp-knitted fabrics and integrate conductive yarns into the loops to achieve desirable sensing performance. [7-9] However, the mechanical non-uniformity and high deformability of knitted loops often cause sensitivity drift, sensing inconsistency, and recovery hysteresis.[10, 11] Coating and dip-treated textile sensors, formed by depositing conductive materials such as carbon nanomaterials, MXenes, metal nanoparticles, or conductive polymers onto fabric surfaces, offer simple processing, broad substrate compatibility, and tunable electrical behavior.[12-14] Yet these sensors generally suffer from poor material adhesion, environmental instability, and mechanical degradation under repeated deformation, which can compromise long-term durability and reduce the intrinsic softness and breathability of the textile substrate.[15, 16] Moreover, the use of multi-material weaving and three-dimensional woven fabrics in sensing textiles provide enhanced dimensional stability, well-defined mechanical responses, and precise control over conductive network layout,[17-21] but the complex preparation processes increase the cost and lead to unexpected manufacturing challenges for sensing textiles.[22-25]

Recently, sewing- and embroidery-based sensors have attracted increasing attention because of their design versatility, rapid fabrication, and seamless integration with garments.[26-28] By programming stitch parameters such as shapes, density, angle, and thread types, conductive pathways can be engineered to achieve localized control over electromechanical properties.[29-31] This approach further benefits from low cost and compatibility with existing textile manufacturing processes.[32] However, most existing designs depend on simple or empirically selected stitch patterns, which leaves the geometric parameter space largely unexplored and hinders a clear understanding of the structure-property relationships governing sensitivity, linearity, and pressure range.[33, 34] The electromechanical reliability of these devices is further limited by the use of coated or chemically modified conductive threads, which are prone to fatigue-induced degradation during repeated loading.[35] In addition, uncontrolled thread tension and the absence of standardized fabrication protocols frequently result in device-to-device inconsistencies, hindering translation to large-area or mass-manufactured wearable systems.[36] Although recent embroidered sensor architectures highlight the potential of programmable stitched networks, they commonly involve multilayer stacking or encapsulation that compromises breathability and complicates integration with everyday textiles.[37, 38] Consequently, a unified, geometry-driven design strategy capable of precisely tailoring the sensing behavior while preserving textile softness and mechanical compliance remains elusive.

© Author(s) 2026. This work is distributed under the Creative Commons BY- 4.0 license:
https://creativecommons.org/licenses/by/4.0/

Textile Science & Research Journal
ISSN: 3059-846X, Volume – 2, Issue – 1, 2026
DOI: https://doi.org/10.63456/tsrj-2-1-35

To address these challenges, we introduce a geometrically programmed stitching framework that leverages stitch geometry to tune the piezoresistive response of textile sensors. By integrating conductive threads with a pressure-sensitive fabric through controlled stitch patterns, the effect of stitch shape, spacing, density, angle, thread type, and the dimensions of the piezoresistive layer on the resistance evolution is investigated. This analysis reveals the structure-performance relationship that enables the predictable, tunable, and scalable design of sensing behaviors. Guided by these insights, we fabricated an optimized stitched sensor exhibiting desirable piezoresistive performance. The resulting device offers a low-cost, customizable, and fully textile-compatible pathway toward next-generation piezoresistive sensors.

2. MATERIALS AND METHODS

2.1 MATERIALS

The piezoresistive textile was fabricated using a 1×1 rib knit composed of a carbon-based conductive nylon yarns (fabric density: 200 courses/10 cm × 130 wales/10 cm). A non-woven felt substrate of thickness in 1 mm was supplied by Daoshenwen Commercial Trading Co., Ltd. (Shaanxi, China). The silver-coated nylon yarn (50 tex) was provided by Techlong Ruifiber Technology Co., Ltd. (Jiangsu, China). A high-strength polyester thread (150D) from Wenzhou Baizhen Thread Co., Ltd. (Zhejiang, China) was employed as the bobbin thread, with a pure cotton sewing thread (60 tex) from Yuanfang Co., Ltd. (Jiangsu, China) serving as the fixed stitching thread.

2.2 PREPARATION OF THE PIEZORESISTIVE TEXTILE SENSOR

The design and fabrication methods of the custom piezoresistive textile sensor are illustrated in Figure 1. The sensor was fabricated using a JUKI HZL-357ZP-C sewing machine (Juki Corporation, China) using selected stitch parameters (Figure 1a). The main fabrication step involves the stitching of conductive yarns onto a layered textile assembly. The commercially available yarns and fabrics (Figure 1b,c) are used as raw materials during this fabrication processes.

The as-prepared sensor was primarily composed of a fabric substrate layer and a piezoresistive fabric layer (Figure 1d). The conductive yarn was engineered to stitch onto the top surface of each of these two fabric layers separately, forming essential electrical pathways. The white fabric substrate provides mechanical support, and the black piezoresistive fabric that acts as the active sensing areas. During the sewing process, the silver-coated nylon conductive yarn was used as the top thread, and the non-conductive polyester thread was used as the bobbin threads. This configuration is crucial as it localizes the conductive pathway to the top surface of each fabric layer, preventing electrical short circuits through the bulk of the material while simultaneously ensuring that the stitches are anchored securely. The final integration of the piezoresistive fabric layer with the underlying fabric substrate was achieved by suturing with the cotton yarn, which provides solid mechanical bonding and maintaining the overall flexibility of the sensor (Figure 1c). This fabrication approach underscores a significant advantage by seamlessly integrating the sensor within textiles, making it highly suitable for wearable electronics and human-machine interaction applications.

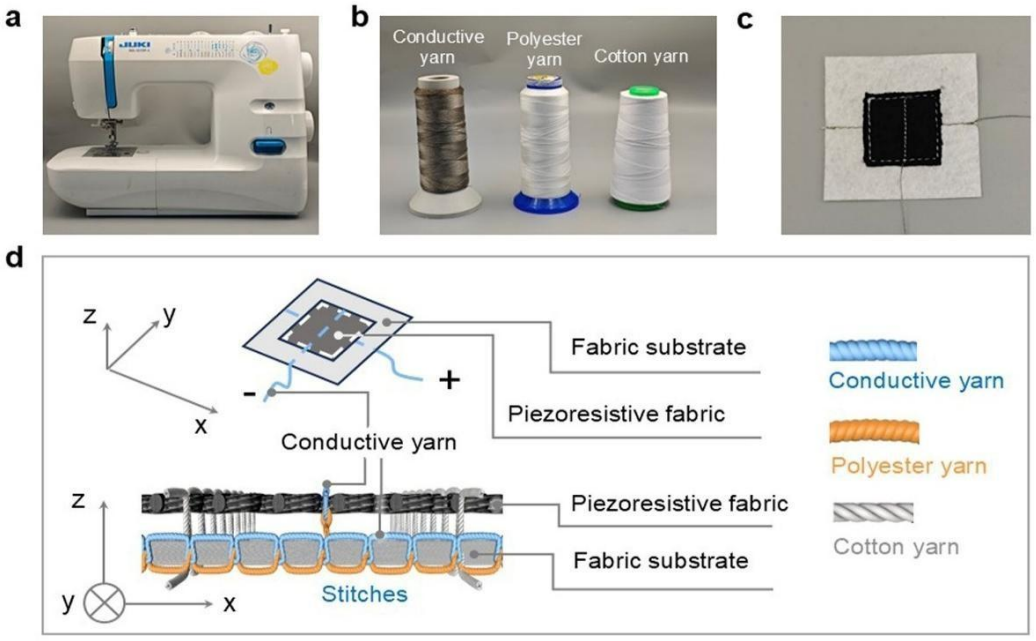

Figure 1. Fabrication and design of the piezoresistive textile sensor. (a) Photo of the sewing machine for fabricating piezoresistive textile sensor. (b) Sewing materials used for making piezoresistive sensor. (c) Photograph of the piezoresistive textile sensor. (d) Schematic illustration of the structure of the piezoresistive sensor.

© Author(s) 2026. This work is distributed under the Creative Commons BY- 4.0 license:
https://creativecommons.org/licenses/by/4.0/

Textile Science & Research Journal
ISSN: 3059-846X, Volume – 2, Issue – 1, 2026
DOI: https://doi.org/10.63456/tsrj-2-1-35

2.3 WORKING PRINCIPLE AND PARAMETER SETTINGS OF THE PIEZORESISTIVE SENSOR

The piezoresistive sensor can reflect the mechanical stress by a quantifiable change in electrical resistance. This behavior is governed by the modulation of internal conductive networks of the piezoresistive fabric under strain, which can be described by a combination of contact mechanics and percolation theory (**Figure 2**).

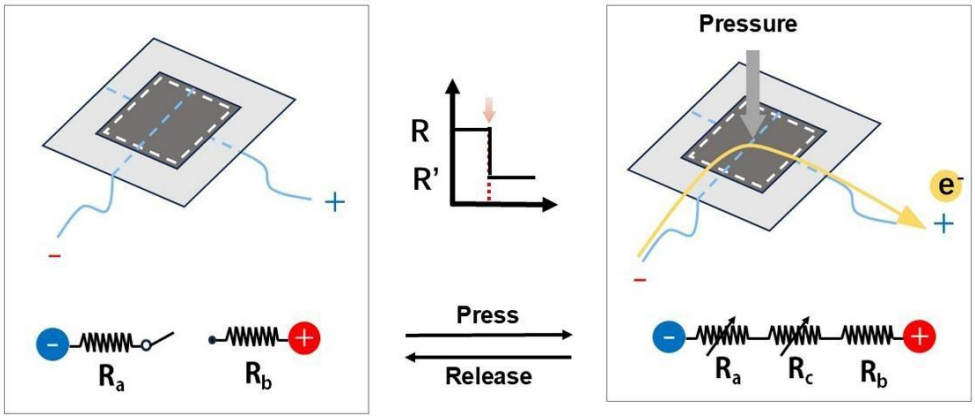

Figure 2. Working principle of the textile piezoresistive sensor.

In the release state, the sensor exhibits a high baseline electrical resistance, R', determined by the intrinsic resistivity of the fabric materials and the limited number of contact points within the piezoresistive fabric. The total resistance can be approximated as the sum of the intrinsic resistance of the conductive yarns, R_{int}, and the constriction resistance at the inter-filament contact points, R_c:

$$R' = R_{int} + \sum_{i=1}^{n} R_{c,i} \qquad (1)$$

where n represents the number of discrete contact points, and $R_{c,i}$ is the resistance of the i^{th} contact point.

Upon applying an external pressure, it induces structural deformation of the fabrics, leading to a significant reduction in the overall electrical resistance, R. Briefly, this reduction stems from two synergistic mechanisms. Firstly, the compressive strain increases the contact points of the fabrics, thereby reducing the constriction resistance. According to the Holm's contact theory, for a single circular contact point, the contact resistance R_c is inversely proportional to the contact radius a:

$$R_c = \frac{\rho}{2a} \qquad (2)$$

where ρ is the resistivity of materials. As pressure increases, the contact radius a grows, leading to a decrease in R_c. Secondly, the deformation creates new conductive pathways by bringing isolated conductive elements into contact, effectively increasing the density of the percolation network. The overall sensor resistance under pressure can thus be modelled as:

$$R = \frac{R_{int} + \sum_{j=1}^{m} R_{c,j}}{K} \qquad (3)$$

where m ($m>n$) is the increased number of contact points under pressure, and K is a factor accounting for the enhanced connectivity and parallel pathways within the network.

The sensitivity S of the sensor, defined as the relative change in resistance per unit pressure P, is therefore a function of these microstructural changes as follows,

$$S = \frac{1}{R'} \frac{\partial(\Delta R)}{\partial P}, \qquad (4)$$

where $\Delta R = R' - R$.

To systematically deconvolute and optimize the effect of the fabrication variables on the sensing performance of the textile sensors, a series of sensors were produced with controlled variations. The specific parameters used in this study are detailed in Table 1.

© Author(s) 2026. This work is distributed under the Creative Commons BY- 4.0 license:
https://creativecommons.org/licenses/by/4.0/

Textile Science & Research Journal
ISSN: 3059-846X, Volume – 2, Issue – 1, 2026
DOI: https://doi.org/10.63456/tsrj-2-1-35

Table 1. Sample dimensions and stitching parameters of the textile sensors

Sewing target	Thread Tension (0-9)	Stitch density (1-4)	Stitch pattern	Stitch width (0-7)	Line spacing (cm)	Object size (cm^2)
Piezoresistive fabric 1	6	2	Straight line	0	Single-line	3 × 3
Piezoresistive fabric 2	6	2	Straight line	0	Single-line	4 × 3
Piezoresistive fabric 3	6	2	Straight line	0	Single-line	5 × 3
Fabric substrate 1	4	1	Straight line	0	Single-line	6 × 6
Fabric substrate 2	4	2	Straight line	0	Single-line	6 × 6
Fabric substrate 3	4	3	Straight line	0	Single-line	6 × 6
Fabric substrate 4	4	4	Straight line	0	Single-line	6 × 6
Fabric substrate 5	6	3	Herringbone	6	Single-line	6 × 6
Fabric substrate 6	6	3	Overlocking	6	Single-line	6 × 6
Fabric substrate 7	6	3	Tree branch	6	Single-line	6 × 6
Fabric substrate 8	6	3	Trapezoid	6	Single-line	6 × 6
Fabric substrate 9	6	3	Fishbone	6	Single-line	6 × 6
Fabric substrate 10	6	2	Herringbone	0	Single-line	6 × 6
Fabric substrate 11	6	2	Herringbone	2	Single-line	6 × 6
Fabric substrate 12	6	2	Herringbone	4	Single-line	6 × 6
Fabric substrate 13	6	2	Herringbone	6	Single-line	6 × 6
Fabric substrate 14	4	3	Straight line	0	Dual-line 0.5	6 × 6
Fabric substrate 15	4	3	Straight line	0	Dual-line 1	6 × 6
Fabric substrate 16	4	3	Straight line	0	Dual-line 1.5	6 × 6
Fabric substrate 17	4	3	Straight line	0	Dual-line 2	6 × 6

2.4 CHARACTERIZATION AND TESTING METHODS OF THE PIEZORESISTIVE SENSOR

The electromechanical characterization of the fabricated piezoresistive sensors was tested using a synchronized setup for applying controlled mechanical stimuli and simultaneously monitoring the corresponding electrical responses. Quasi-static pressure was applied normal to the sensor surface using a mechanical tester (YG008E, Wenzuan Darong Textile Instrument Co., Ltd., China). To ensure precise calibration and a broad dynamic range, a series of weights (2, 5, 10, 20, 50, and 100 g) were employed, enabling the application of well-defined pressures across multiple orders of magnitude. The resultant resistance signal of the sensor was recorded using a high-precision digital multimeter (DMM6500, Keithley). This experimental configuration allowed for the direct correlation of the applied mechanical load with the transient and steady-state electrical output, facilitating the accurate assessment of key performance metrics, including sensitivity, hysteresis, and response time.

3. RESULTS AND DISCUSSION

3.1 EFFECT OF STITCH DENSITY

For sewing-stitch textile sensors, the sensing performance is tailored by the manufacturing parameters of the sewing process. The configuration of the conductive yarn, specifically the density of the stitches, directly determine the initial conductive network density and its mechanical and electronic responses. Figure 3a illustrates different stitch densities, namely 3, 6, 9, and 12 per cm. At low densities, stitches remain widely spaced, enabling pronounced local deformation of the textile substrate and substantial modulation of inter-fiber contact under load. At higher densities, the stitched network becomes more continuous, with reduced inter-stitch spacing and stronger mechanical coupling, thereby restricting out-of-plane deformation and redefining the deformation field that drives resistance change.

© Author(s) 2026. This work is distributed under the Creative Commons BY- 4.0 license:
https://creativecommons.org/licenses/by/4.0/

Textile Science & Research Journal
ISSN: 3059-846X, Volume – 2, Issue – 1, 2026
DOI: https://doi.org/10.63456/tsrj-2-1-35

To analyze the sensing performance, the relative resistance change ($\Delta R/R_0$) and response time of the textile sensors were characterized. The $\Delta R/R_0$ is calculated based on the initial resistance R_0 at zero pressure and the change value ΔR under a pressure of 1.25 kPa. As shown in Figure 3b, the value of $\Delta R/R_0$ shows a clear density-dependent trend, and it reduces from 137 to 95 when the stitch density increases from 3 to 12 per centimeter. Higher densities introduce more conductive overlaps and parallel microcontacts, lowering the baseline resistance R_0. Piezoresistive sensitivity is mainly determined by the deformation of a limited number of microcontacts; once the conductive network becomes sufficiently dense, additional deformation yields only small variations in total resistance. As a result, $\Delta R/R_0$ decreases monotonically with the increase of the stitch density, marking a transition from a deformation-dominated to a conduction-saturated condition. The stitch density shows relatively small effect on the response time of the textile sensors at low densities; however, a high density at 12 stitches per centimeter induces a decrease in response time (Figure 3c). This can be caused by the fact that the high density enhances lateral constraints and increases inter-fiber friction in conductive yarns, which decreases the yarn elasticity and viscoelastic dissipation in the compression process, and thus reduces the hysteresis.

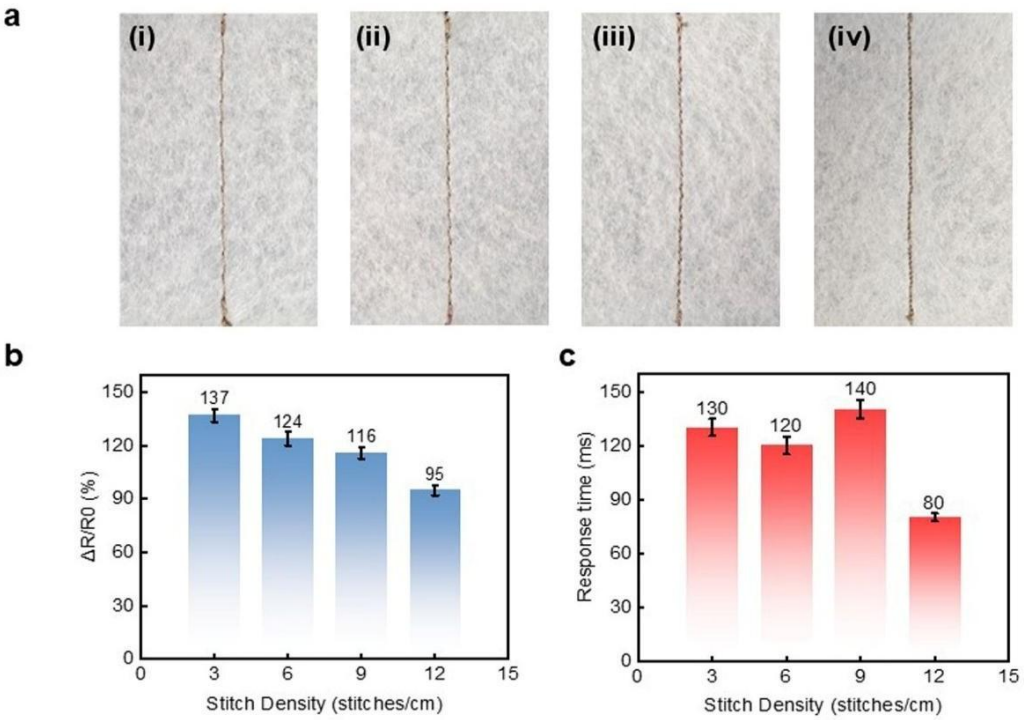

Figure 3. Effects of stitch density on the sensing properties of the piezoresistive sensors. Each performance at each density level was tested ten times, and the average value with standard deviations was reported. (a) Schematic illustration of the optical images for textile sensors with stitch densities of 3, 6, 9, and 12 stitches per centimeter. (b) Relative resistance changes as a function of stitch density between applied pressures of 0 and 1.25 kPa. (c) Sensor response time versus stitch density upon applying a pressure of 1.25 kPa.

3.2 EFFECT OF STITCH PATTERNS

Stitch patterns govern local stiffness and strain distribution, thereby affecting the evolution of fiber contact within the fabrics and the resulting electrical sensing performance. As shown in Figure 4a, the five representative patterns exhibit different symmetry, branching density, and interlocking configurations, which in turn shape the formation and modulation of conductive contact networks upon loading. Oblique or branched paths, such as Herringbone and Branch stitch introduce multi-directional deformation modes that enhance contact variation, leading to larger relative resistance changes in the value of the $\Delta R/R_0$. In contrast, linear or ladder-like designs of the Overlocking and Trapezoid constrain deformation along a primary axis, producing simpler strain fields and smaller $\Delta R/R_0$ values.

As shown in Figure 4b, the Herringbone configuration yields the highest $\Delta R/R_0$ (82%) among all patterns due to its angled V-shaped geometry that has relatively large conductive pathway, thereby amplifying microcontact modulation. The Trapezoid pattern exhibits the lowest sensitivity with a value of 69% because its nearly linear, periodic structure reduce the length of conductive pathway and suppresses contact evolution. Overlocking and Fishbone structures show intermediate $\Delta R/R_0$ values of 75% and 70%, where their interlocked features increase contact density but distribute deformation more evenly, preventing strong strain localization. The Tree-branch pattern (77%), characterized by asymmetric lateral bifurcation, generates heterogeneous strain fields and provides moderate contact amplification. Overall, patterns incorporating oblique or branched elements facilitate distributed deformation and more dynamic contact reconfiguration,

© Author(s) 2026. This work is distributed under the Creative Commons BY- 4.0 license:
https://creativecommons.org/licenses/by/4.0/

Textile Science & Research Journal
ISSN: 3059-846X, Volume – 2, Issue – 1, 2026
DOI: https://doi.org/10.63456/tsrj-2-1-35

whereas linear arrangements impose directional stiffness that limits contact evolution, thereby establishing a clear link between stitch geometry and sensing performance.

In contrast, the response time exhibits a trend opposite to that of the relative resistance change (Figure 4c). The Herringbone pattern shows the fastest response with response time of 131 ms. By comparison, the Trapezoid and Overlocking patterns display longer response times (180 ms and 171 ms). The Tree-branch structure showing response time of 150 ms demonstrates intermediate behavior, balancing localized strain concentration with frictional dissipation along its branching nodes. These results indicate that geometric architecture governs deformation anisotropy, contact-network evolution, and energy-dissipation mechanisms, thereby producing distinct functional responses. Consequently, geometric programming serves as a key design dimension for tailoring textile-sensor performance beyond material composition alone.

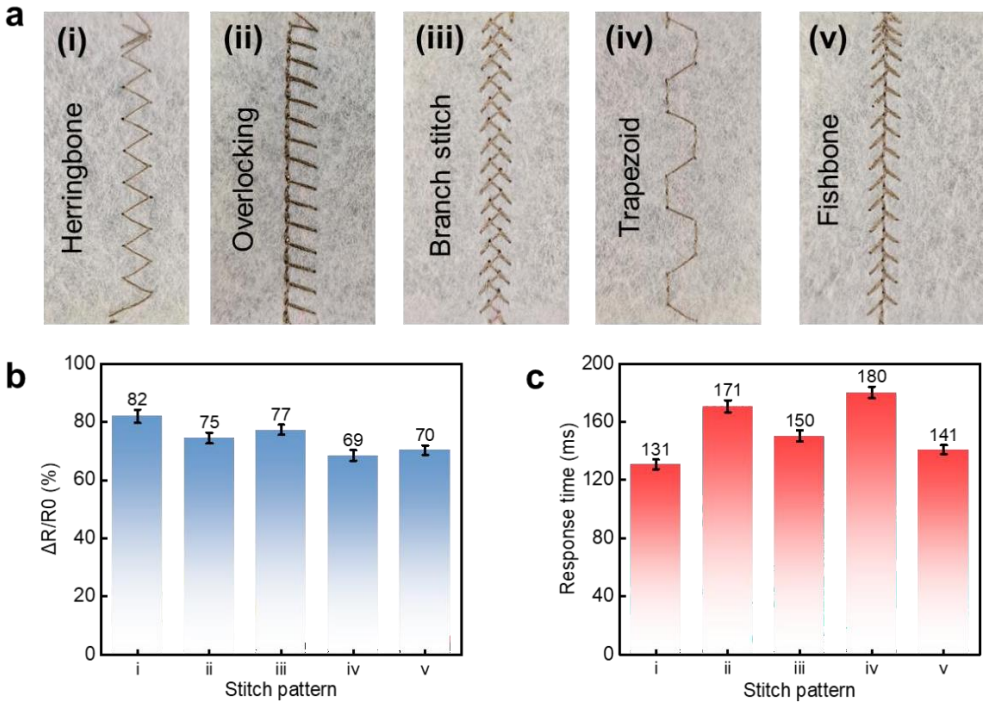

Figure 4. Effects of stitch pattern on the sensing properties of the piezoresistive sensor. (a) Schematic illustration of the sensors fabricated with different stitch patterns. (b) Relative resistance change of sensors with different stitch patterns under 4 kPa applied pressure. (c) Response time versus stitch pattern under 4 kPa applied pressure.

3.3 EFFECT OF THE STITCH ANGLES

The structural influence of the herringbone stitch vertex angle, θ on sensor performance is quantified in Figure 5. Four representative angles, namely 40°, 70°, 100°, and 180°, were selected, and the geometric evolution from sharp and highly folded zigzag motifs (40°), to moderately open structures (70° and 100°), and ultimately to a fully linear seam at 180° (Figure 5a). This structural progression leads to distinct trends in sensing sensitivity, as quantified by the relative resistance change ($\Delta R/R_0$) in Figure 5b. The sensitivity increases steadily with vertex angle, from 86% at θ = 40° to approximately 95% at θ = 180°. This trend is governed by the stitch geometry pathway and microcontact activation pattern under compression. As the angle changes from 70° to 100°, the zigzag structure becomes open. A smaller-angle zigzag structure may exhibit a larger initial contact area, potentially yielding a lower baseline resistance R_0. More importantly, the initial contacts for small-angle zigzag structure modulates conductive contacts within narrow apex regions, failing to engage the broader conductive network effectively. The resulting limited increase in conductive paths produces a small absolute resistance change (ΔR), leading to lower relative sensitivity ($\Delta R/R_0$). In the linear configuration (θ = 180°), the seam deforms through uniform axial compression, which promotes continuous and synchronized evolution of conductive contacts along the entire stitch line with a relatively low R_0. Despite the absence of zigzag-induced contact reconfiguration, this uniform deformation footprint maximizes the participation of the conductive network, resulting in the highest observed sensitivity ($\Delta R/R_0 \approx 95\%$).

The dynamic response characteristics reveal an inverse correlation with the sensitivity trend (Figure 5c), where the sensor's response time drops markedly as the vertex angle increases from 220 ms at 40° to 110 ms at 180°. This acceleration in recovery can be attributed to the reduction of internal mechanical dissipation. Structures with small angles exhibit pronounced friction and viscoelastic hysteresis, as their sharp folds resist smooth unfolding during load release, thereby delaying the separation of microcontacts. In contrast, larger-angle configurations facilitate more elastic deformation, with diminished geometric locking and friction, leading to quicker mechanical relaxation. The straight stitch (θ = 180°), entirely free of lateral folds, demonstrates the fastest recovery due to its purely axial deformation mode. Figure 5d quantifies the

© Author(s) 2026. This work is distributed under the Creative Commons BY- 4.0 license:
https://creativecommons.org/licenses/by/4.0/

Textile Science & Research Journal
ISSN: 3059-846X, Volume – 2, Issue – 1, 2026
DOI: https://doi.org/10.63456/tsrj-2-1-35

minimum trigger force needed to initiate a detectable resistance change. This threshold force rises substantially with the vertex angle, from 3.5 mN at 40° to 100 mN at 180°, reflecting a direct correspondence between stitch geometry and structural stiffness. The structure with an angle of 40° deforms easily under light loading, promptly engaging the conductive network, whereas the linear seam of 180° requires considerably higher compressive force to achieve the same level of microcontact activation. This demonstrates structure-function relationship and underscores "angle engineering" as a potential and materials-agnostic strategy for designing textile sensors.

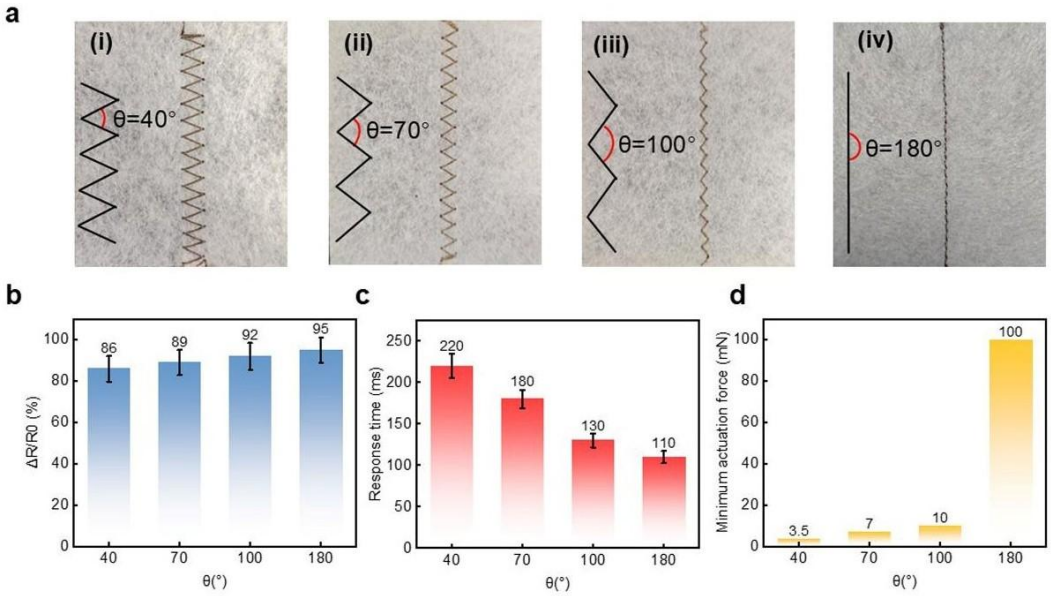

Figure 5. Effect of the herringbone stitch angle on the sensing properties of the piezoresistive sensor. (a) Schematic illustration of sensors fabricated with different herringbone stitch angles (θ = 40°, 70°, 100°, and 180°). (b) Relative resistance change as a function of herringbone stitch angle under 4 kPa applied pressure. (c) Sensor response time versus herringbone stitch angle under 4 kPa applied pressure. (d) Minimum trigger force as a function of the herringbone stitching angle.

3.4 EFFECT OF THE STITCH SPACING

The geometric programming of piezoresistive sensors extends to the critical parameter of stitch spacing, which governs the spatial distribution of conductive pathways across the sensing area. As systematically compared in Figure 6a, we fabricated sensors with four distinct stitch spacings (0.5, 1.0, 1.5, and 2.0 cm) while maintaining identical materials and other manufacturing parameters. All electromechanical characterizations were performed under 4 kPa applied pressure, with data points representing means from ten independent measurements.

Analysis of the relative resistance change ($\Delta R/R_0$) reveals a clear monotonic relationship with stitch spacing (Figure 6b). The maximum response (~143%) is achieved at the narrowest spacing of 0.5 cm, where the high density of conductive pathways enables efficient formation of microcontacts under compression. As the spacing increases to 1.0 cm, $\Delta R/R_0$ decreases to ~129%, indicating reduced network connectivity. This declining trend continues with wider spacings, reaching ~113% at 1.5 cm and ~104% at 2.0 cm, which demonstrates that the increase of separation spaces between stitch lines diminishes the piezoresistive response. In contrast, the dynamic response characteristics show a distinct pattern, as shown in Figure 6c. Response times are relatively stable, maintaining values of approximately 130-140 ms across all spacing configurations. Specifically, the response time measures ~130 ms at 0.5 cm spacing, increases slightly to ~140 ms at 1.0 cm spacing, returns to ~130 ms at 1.5 cm spacing, and settles at ~140 ms at 2.0 cm spacing. This stability suggests that the temporal response is primarily governed by the intrinsic viscoelastic properties of the textile substrate and the fundamental contact mechanics, rather than being significantly influenced by variations in stitch spacing. These demonstrate that stitch spacing serves as a crucial parameter for modulating sensor sensitivity while maintaining consistent dynamic performance. The strong dependence of $\Delta R/R_0$ on spacing highlights the importance of conductive pathway density in determining piezoresistive response, whereas the relative invariance of response time indicates that temporal characteristics can be optimized independently. This decoupling of static and dynamic performance metrics provides valuable flexibility for designing textile sensors tailored to specific application requirements.

© Author(s) 2026. This work is distributed under the Creative Commons BY- 4.0 license:
https://creativecommons.org/licenses/by/4.0/

Textile Science & Research Journal
ISSN: 3059-846X, Volume – 2, Issue – 1, 2026
DOI: https://doi.org/10.63456/tsrj-2-1-35

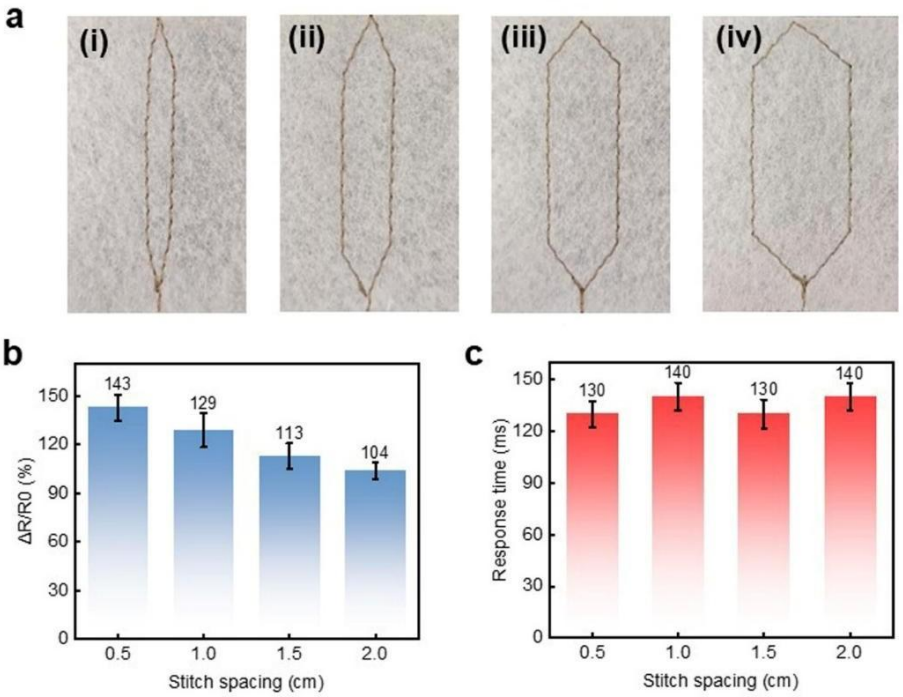

Figure 6. Effect of stitch spacing on the sensing properties of the piezoresistive sensor. (a) Schematic illustration of textile sensors with different stitch spacings. (b) Relative resistance change as a function of stitch spacing under 4 kPa applied pressure. (c) Response time versus stitch spacing under applied pressure of 4 kPa.

3.5 EFFECT OF THE LINEAR DENSITY OF CONDUCTIVE YARNS

The linear density of conductive yarns is also an important factor that affects the electromechanical behavior of piezoresistive textile sensors. As shown in Figure 8a, three distinct silver-coated nylon yarn variants were meticulously selected to establish a comprehensive parameter matrix (Table 2), with each experimental data point representing the mean of ten independent measurements to ensure statistical significance. The detailed characterization summarized in Table 3, which further reveals the interplay among multiple material parameters. With the increase of the linear density from 41.68 tex to 99.36 tex, the electrical resistivity decreases from 200 Ω/cm to 15 Ω/cm. The mechanical properties exhibit nonlinear relationship, with breaking elongation showing an initial increase from 24.5% to 27.2% followed by a decrease to 15%, and tensile strength demonstrating a significant enhancement from 10.38 to 21.34 N across the yarn series.

The yarn twist level (ranging from 400 to 800 TPM) emerges as a pivotal structural parameter that orchestrates both electrical and mechanical performance. Higher twist density in yarn 3 creates a compact architecture that optimizes inter-filament electrical contact, contributing to its superior conductivity, while simultaneously increasing yarn stiffness and reducing breaking elongation. This twist-mediated structural organization creates a fundamental trade-off: enhanced electrical pathways come at the expense of mechanical compliance, directly influencing the yarn's ability to conform to the piezoresistive fabric under loading conditions.

The quasi-static performance analysis in Figure 8b demonstrates a remarkable correlation between material properties and sensing sensitivity. The relative resistance change ($\Delta R/R_0$) progresses from 94% to 97% and reaches 100% for yarns 1-3 respectively under 4 kPa pressure. This enhancement derives from a synergistic mechanism where reduced electrical resistivity minimizes series resistance, while optimized mechanical properties, particularly the balanced combination of moderate tensile strength (8.82 N) and superior breaking elongation (27.2%) in yarn 2, facilitate optimal interfacial contact evolution with the piezoresistive layer.

Dynamic response characterization of the sensors also reveals a nonlinear relationship with material parameters (Figure 8c). The improvement in response time from 190 ms to 150 ms between yarn 1 and yarn 2 correlates with enhanced conductivity and mechanical compliance. However, the identical response times of yarn 2 and yarn 3, despite they have different twist levels and mechanical properties. Moreover, microstructural analysis confirms that yarn selection represents a multi-objective optimization challenge. While yarn 2 demonstrates favorable mechanical compliance, its moderate resistivity ultimately limits the achievable sensitivity. Yarn 1's combination of high resistivity and intermediate mechanical properties results in suboptimal performance across both static and dynamic metrics. Yarn 3 emerges as the optimal solution, achieving exceptional sensitivity through its superior conductivity and compact structure, while its mechanical characteristics, including high tensile strength and controlled stiffness, prove advantageous for maintaining stable interfacial contact and long-term reliability under cyclic loading conditions.

© Author(s) 2026. This work is distributed under the Creative Commons BY- 4.0 license:
https://creativecommons.org/licenses/by/4.0/

Textile Science & Research Journal
ISSN: 3059-846X, Volume – 2, Issue – 1, 2026
DOI: https://doi.org/10.63456/tsrj-2-1-35

Table 2. Sewing parameters of different conductive yarns

Material type	Sewing target	Thread Tension (0-9)	Stitch density (1-4)	Stitch pattern	Stitch width (0-7)	Line spacing (cm)	Object size (cm^2)
Silver-plated nylon 2	Piezoresistive fabric	6	2	Straight line	0	Single-line	3 × 3
Silver-plated nylon 1	Fabric substrate 1	4	3	Straight line	0	Single-line	6 × 6
Silver-plated nylon 2	Fabric substrate 2	4	3	Straight line	0	Single-line	6 × 6
Silver-plated nylon 3	Fabric substrate 3	4	3	Straight line	0	Single-line	6 × 6

Table 3. Performance comparisons of different conductive yarns

Material type	Linear density (tex)	Diameter (mm)	Resistivity(Ω/cm)	Tensile strength (N)	breaking elongation（%）	Twist (turn/m)
Silver-plated nylon 1	41.68	0.2	200	10.38	24.5	400
Silver-plated nylon 2	50.59	0.3	100	8.82	27.2	600
Silver-plated nylon 3	99.36	0.5	15	21.34	15	800

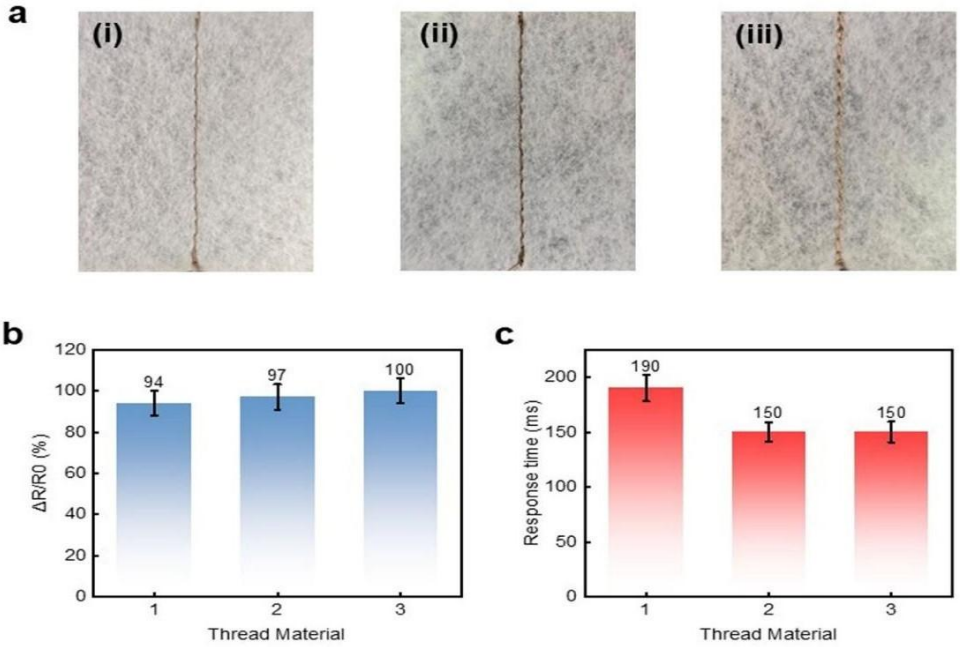

Figure 7. Influence of conductive yarn types on the sensing properties of the piezoresistive sensor. (a) Optical images of sensors fabricated with different conductive yarn types. (b) Relative resistance changes of textile sensors with different conductive yarns upon applying 4 kPa pressure. (c) Response time of the textile sensors upon applying 4 kPa pressure.

3.6 EFFECT OF THE DIMENSIONS OF PIEZORESISTIVE FABRICS

The influence of piezoresistive fabric dimensions on the sensing response was examined by extending the active piezoresistive sensing region from 3 to 5 cm in length while keeping the width and stitching parameters fixed (Figure 8a). The measurements indicate a length-dependent response of the resistance. Increasing the effective gauge length enlarges the deformable conductive network, thereby altering the distribution of current-carrying pathways and modifying how strain is transferred through the textile matrix during loading. As the sensing region increases from 3 to 5 cm, the relative resistance change, $\Delta R/R_0$, rises nonlinearly from 82% at 3 cm to 123% at 4 cm, ultimately reaching 150% at 5 cm (Figure 8b). This can be attributed to the fact that increasing piezoresistive fabric dimension causes the enhancement in the possible changes of contact points and conductive networks upon compression. At 3 cm, the shorter gauge length reduces opportunities for microcontact generation and limiting resistance variation. When extended to 4 cm, the fabric exhibits greater mechanical

© Author(s) 2026. This work is distributed under the Creative Commons BY- 4.0 license:
https://creativecommons.org/licenses/by/4.0/

Textile Science & Research Journal
ISSN: 3059-846X, Volume – 2, Issue – 1, 2026
DOI: https://doi.org/10.63456/tsrj-2-1-35

compliance, enabling more pronounced buckling and an increased density of conductive contact points. At the maximum length of 5 cm, the deformable network reaches a regime where both the number of active conductive pathways and their collective deformation are optimized, yielding the most efficient conversion of applied strain into electrical resistance changes.

The response time shows an inverse dependence on fabric length (Figure 8c). Increasing the active length from 3 to 5 cm leads to a substantial reduction in response time, decreasing from 210 ms to 120 ms and further to 80 ms. This trend contrasts with conventional expectations for longer sensing elements. The observed acceleration in response time can be attributed to the reduced bending stiffness and more uniform stress distribution in longer fabric segments, which lessen localized strain and viscoelastic effects. In addition, the enlarged conductive network facilitates faster stabilization of electrical contacts. Thus, these factors enable quicker transitions between conductive states. Overall, fabric length is identified as a critical geometric parameter governing the sensor's performance. Length optimization in this study yields an 83% increase in $\Delta R/R_0$ alongside a 62% decrease in response time, demonstrating its strong influence on both static sensitivity and dynamic behavior.

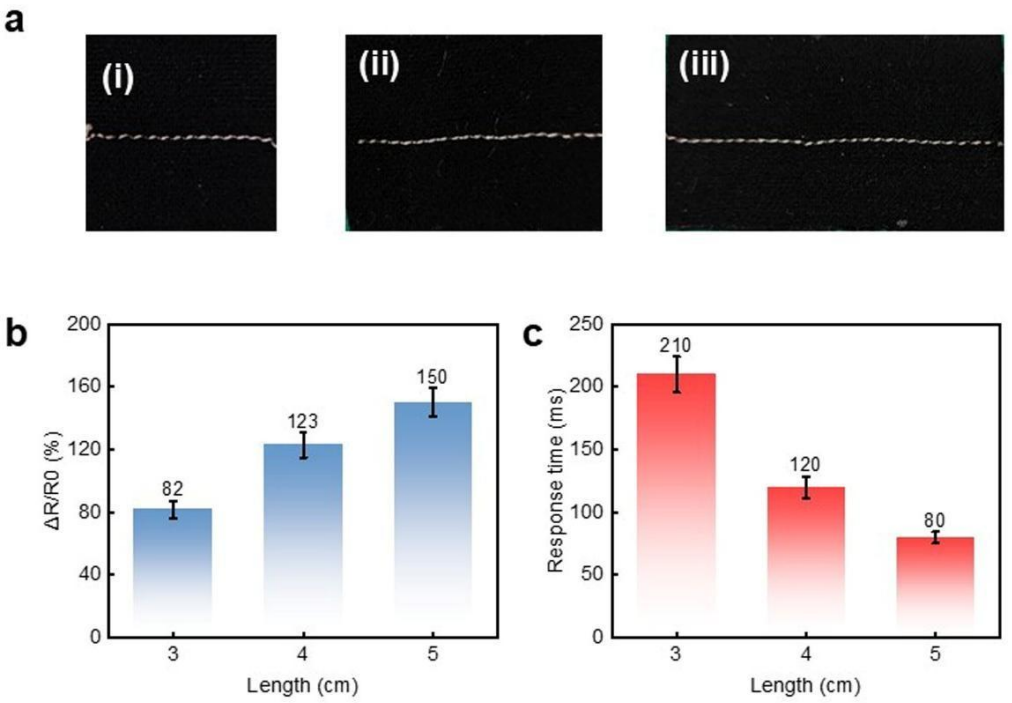

Figure 8. Influence of piezoresistive fabric length on the sensing properties of the piezoresistive sensors. (a) Optical images of sensors fabricated with different piezoresistive fabric lengths. (b) Relative resistance change as a function of piezoresistive fabric length under 4 kPa applied pressure. (c) Sensor response time versus piezoresistive fabric length under 4 kPa applied pressure.

3.7 PERFORMANCE VALIDATION OF THE OPTIMIZED PIEZORESISTIVE SENSOR

The optimized piezoresistive textile sensor was developed by integrating the effective geometric and stitching parameters identified above. As summarized in Table 4, the final configuration incorporates a highly conductive silver-coated nylon yarn, a moderately compliant 3 × 5 cm piezoresistive fabric layer, balanced stitch density on the sensing side, and a dual-line 0.5 cm Herringbone pattern on the substrate. A stitch angle of 100° was selected because it provides a balanced trade-off among the examined geometries, offering high sensitivity and fast response while requiring a lower activation force than the 180° linear configuration. This coordinated selection of stitched geometries can yield a hierarchical structure that enhances strain propagation, promote cooperative microcontact evolution, and stabilize the conductive pathways under repeated deformation. The structural layout is shown in Figure 9a, and the assembled device is presented in Figure 9b.

The optimized sensor exhibits desirable pressure sensitivity, characterized by three distinct linear regimes with the gauge factor (GF) ranging from 3.4% kPa^{-1} to 0.09% kPa^{-1} (Figure 9c). The moderate stitch density allows microcontacts to activate progressively at low pressures; the Herringbone architecture redistributes strain along multiple angled pathways, enabling cooperative deformation at intermediate loads; and the compact, high-twist conductive yarn supports stable contact convergence when higher pressures compress the sensing network more fully. Dynamic response time tests further highlight the advantages of this integrated design. As shown in Figure 9d, the sensor demonstrates rapid, repeatable transitions between compressed and relaxed states, with minimal hysteresis and viscoelastic delay. This behavior directly reflects the optimized balance between yarn stiffness, stitch-induced constraint, and substrate compliance. The engineered structure facilitates prompt microcontact reorganization during transient loading, avoiding the energy losses typically associated with

© Author(s) 2026. This work is distributed under the Creative Commons BY- 4.0 license:
https://creativecommons.org/licenses/by/4.0/

Textile Science & Research Journal
ISSN: 3059-846X, Volume – 2, Issue – 1, 2026
DOI: https://doi.org/10.63456/tsrj-2-1-35

overly rigid stitch patterns or poorly matched yarn mechanics. Long-term cycling stability was evaluated under cyclic loading and unloading between 1 kPa and 0 kPa (Figure 9e). The sensor shows consistent resistance responses over 3000 cycles. This durability arises from the interplay of several design factors. First, the high-twist conductive yarn can preserve inter-filament contact integrity; second, the Herringbone stitches distribute deformation uniformly, preventing local mechanical fatigue; and the dual-line spacing stabilizes the global deformation field, reducing creep and structural drift. The combined effect ensures that the conductive network remains mechanically and electrically reliable during prolonged use.

The sensor's response under constant and stepwise pressures further validates its functional robustness, as shown in Figure 10. Under constant 4 kPa loading, the resistance signal remains stable with negligible drift, illustrating excellent resistance to creep and long-term relaxation (Figure 10a). The low hysteresis (<3%) shown in Figure 10b also demonstrates the reversibility of the sensing mechanism. The loading and unloading curves exhibit only small deviations, which reflects minimal viscoelastic loss and highly repeatable microcontact evolution. In stepwise loading experiments (Figure 10c), the device exhibits sharply defined and non-overlapping resistance plateaus, indicating precise pressure discriminability and a high signal-to-noise ratio. These outcomes confirm that the optimized geometric architecture produces a predictable scaling of microcontact activation in response to incremental pressure changes.

Overall, the performance validation demonstrates that the optimized sensor achieves a synergistic enhancement in sensitivity, response speed, stability, and pressure resolution. The results underscore the power of geometric programming as a design paradigm capable of delivering textile sensors with tunable and highly reliable electromechanical properties.

Table 4. Sewing parameters for the optimized piezoresistive sensor.

Sewing target	Conductive yarn material	Thread Tension (0-9)	Stitch density (1-4)	Stitch pattern	Stitch width (0-7)	Line spacing (cm)	Object size(cm^2)
Piezoresistive fabric	2	6	2	Straight line	0	Single-line	3 × 5
Fabric substrate	3	6	4	Herringbone	2	Dual-line 0.5	6 × 6

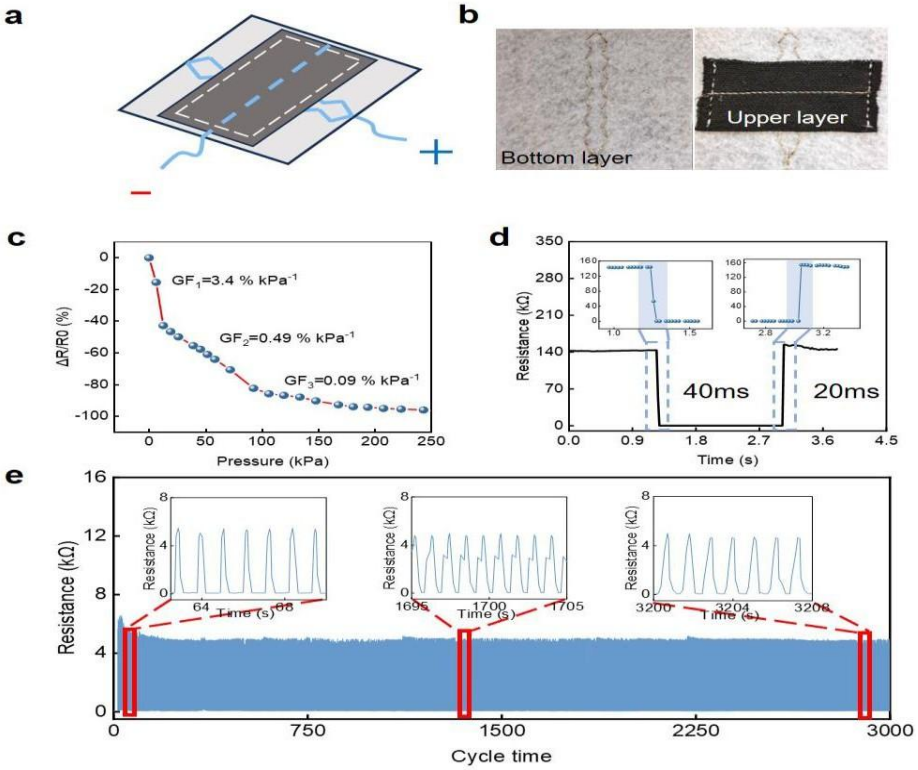

Figure 9. Sensing performance of the optimized piezoresistive textile sensor. (a) Design diagram of the piezoresistive sensor. (b) Photograph of the fabricated sensor. (c) Relative resistance change ($\Delta R/R_0$) as a function of applied pressures. (d) Real-time resistance response under dynamic loading, showing rapid response and recovery. (e) Cyclic stability under 1 kPa for 3000 cycles, indicating robust performance and long-term durability.

© Author(s) 2026. This work is distributed under the Creative Commons BY- 4.0 license:
https://creativecommons.org/licenses/by/4.0/

Textile Science & Research Journal
ISSN: 3059-846X, Volume – 2, Issue – 1, 2026
DOI: https://doi.org/10.63456/tsrj-2-1-35

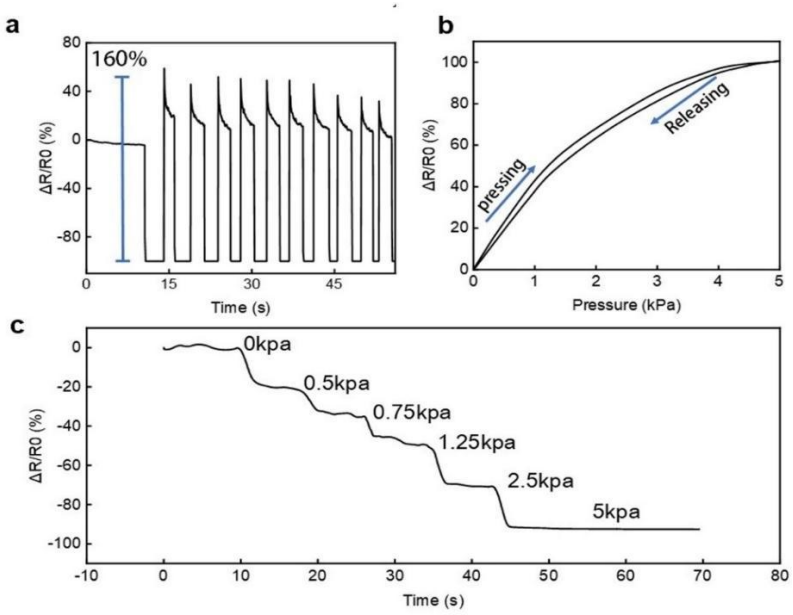

Figure 10. Sensor response to constant and stepwise pressures. (a) Relative resistance change ($\Delta R/R_0$) under a constant 4 kPa pressure. (b) Hysteresis of the piezoresistive sensor by a cycle of pressing and releasing tests. (c) Stepwise resistance changes in response to graded pressures.

4. CONCLUSION

This work develops a geometrically programmed stitching strategy for creating textile-based piezoresistive sensors with tunable electromechanical properties. By decoupling the effects of stitch angle, density, spacing, and dimensions, we clarify the relationships among geometric parameters, strain redistribution, microcontact evolution, and signal stability within textile structures. Integrating the optimized parameters into a unified design yields a textile sensor with high sensitivity, fast dynamic response, low hysteresis and long-term durability. Moreover, the study demonstrates that stitch geometry serves not only as a structural feature but also as a programmable design variable capable of directing pressure-transduction pathways and enabling predictable sensing performance. This geometry-driven approach offers a practical framework for engineering next-generation textile sensors that are both mechanically robust and structurally adaptive, providing a foundation for scalable, and pattern-informed sensing systems for potential applications in wearable electronics, human-machine interfaces, and soft robotics.

CONFLICT OF INTEREST

The authors declare no conflict of interest.

REFERENCES

[1] APTABUSJAMAN M, ISLAM S R, SADANNAVAR M K, et al. Textile based pressure sensors: a review of materials, fabrication, and applications [J]. The Journal of The Textile Institute, 2025, 116(11): 2791-813.
[2] LI J, FANG L, SUN B, et al. Review—Recent Progress in Flexible and Stretchable Piezoresistive Sensors and Their Applications [J]. Journal of The Electrochemical Society, 2020, 167(3).
[3] FIORILLO A S, CRITELLO C D, PULLANO S A. Theory, technology and applications of piezoresistive sensors: A review [J]. Sensors and Actuators A: Physical, 2018, 281: 156-75.
[4] GEORGOPOULOU A, CLEMENS F. Piezoresistive Elastomer-Based Composite Strain Sensors and Their Applications [J]. ACS Applied Electronic Materials, 2020, 2(7): 1826-42.
[5] YANG Y, LIU Y, YIN R. Fiber/Yarn and Textile-Based Piezoresistive Pressure Sensors [J]. Advanced Fiber Materials, 2024, 7(1): 34-71.
[6] CHOI M, VU C C, KIM J. Effects of Ag-coated twisted-yarns and equivalent circuits on textile pressure sensors [J]. Sensors and Actuators A: Physical, 2021, 332.
[7] LIN X, SEET B-C. A Linear Wide-Range Textile Pressure Sensor Integrally Embedded in Regular Fabric [J]. IEEE Sensors Journal, 2015, 15(10): 5384-5.
[8] KIM G, VU C C, KIM J. Single-Layer Pressure Textile Sensors with Woven Conductive Yarn Circuit [J]. Applied Sciences, 2020, 10(8).
[9] WANG L, TIAN M, QI X, et al. Customizable Textile Sensors Based on Helical Core-Spun Yarns for Seamless Smart Garments [J]. Langmuir, 2021, 37(10): 3122-9.
[10] XIE J, PAN S, ZHANG Y, et al. knitted fabric-based flexible piezoresistive pressure sensors for human monitoring and underwater emergency rescue [J]. Sensors and Actuators A: Physical, 2025, 382.

© Author(s) 2026. This work is distributed under the Creative Commons BY- 4.0 license:
https://creativecommons.org/licenses/by/4.0/

[11] WARNCKE M N, BOHMER C H, SACHSE C, et al. Advancing Smart Textiles: Structural Evolution of Knitted Piezoresistive Strain Sensors for Enabling Precise Motion Capture [J]. Polymers (Basel), 2023, 15(19).
[12] LI K, YANG W, SHEN Z, et al. Flexible graphene pressure sensor based on sponge sewn with cotton [J]. Sensors and Actuators A: Physical, 2023, 354.
[13] ABDUL SAMAD Y, KOMATSU K, YAMASHITA D, et al. From sewing thread to sensor: Nylon® fiber strain and pressure sensors [J]. Sensors and Actuators B: Chemical, 2017, 240: 1083-90.
[14] WANG Y, YUE Y, CHENG F, et al. Ti(3)C(2)T(x) MXene-Based Flexible Piezoresistive Physical Sensors [J]. ACS Nano, 2022, 16(2): 1734-58.
[15] KHALIFA M, WUZELLA G, LAMMER H, et al. Smart paper from graphene coated cellulose for high-performance humidity and piezoresistive force sensor [J]. Synthetic Metals, 2020, 266.
[16] ALTAF M, REHMAN B, REHMAN A, et al. Ultrasensitive piezoresistive strain sensors based on CNTs/Ag-NPs coated highly stretchable textile [J]. Journal of Materials Science: Materials in Electronics, 2020, 31(12): 9870-7.
[17] GAO L, ZHU C, LI L, et al. All Paper-Based Flexible and Wearable Piezoresistive Pressure Sensor [J]. ACS Appl Mater Interfaces, 2019, 11(28): 25034-42.
[18] GU M, ZHOU X, SHEN J, et al. High-sensitivity, ultrawide linear range, antibacterial textile pressure sensor based on chitosan/MXene hierarchical architecture [J]. iScience, 2024, 27(4): 109481.
[19] LAI C, WU X, HUANG C, et al. Fabrication and performance of full textile-based flexible piezoresistive pressure sensor [J]. Journal of Materials Science: Materials in Electronics, 2022, 33(8): 4755-63.
[20] LIU M, PU X, JIANG C, et al. Large-Area All-Textile Pressure Sensors for Monitoring Human Motion and Physiological Signals [J]. Adv Mater, 2017, 29(41).
[21] LOU M, ABDALLA I, ZHU M, et al. Hierarchically Rough Structured and Self-Powered Pressure Sensor Textile for Motion Sensing and Pulse Monitoring [J]. ACS Appl Mater Interfaces, 2020, 12(1): 1597-605.
[22] WU R, MA L, BALKRISHNA PATIL A, et al. A facile method to prepare a wearable pressure sensor based on fabric electrodes for human motion monitoring [J]. Textile Research Journal, 2019, 89(23-24): 5144-52.
[23] ZHANG Q, SONG H, ZOU P, et al. Flame retardant flexible pressure sensor textile based on T-ZnO [J]. Materials Today Nano, 2025, 32.
[24] ZHOU Y, ZHAO L, TAO W, et al. All-Nanofiber Network Structure for Ultrasensitive Piezoresistive Pressure Sensors [J]. ACS Appl Mater Interfaces, 2022, 14(17): 19949-57.
[25] ZHOU Z, LI Y, CHENG J, et al. Supersensitive all-fabric pressure sensors using printed textile electrode arrays for human motion monitoring and human–machine interaction [J]. Journal of Materials Chemistry C, 2018, 6(48): 13120-7.
[26] CHOUDHRY N A, SHEKHAR R, RASHEED A, et al. Effect of Conductive Thread and Stitching Parameters on the Sensing Performance of Stitch-Based Pressure Sensors for Smart Textile Applications [J]. IEEE Sensors Journal, 2022, 22(7): 6353-63.
[27] JANG J, KIM J. Prediction of Electrical Resistance with Conductive Sewing Patterns by Combining Artificial Neural Networks and Multiple Linear Regressions [J]. Polymers (Basel), 2023, 15(20).
[28] MALEK A S, ELNAHRAWY A, WAGDY D. Electrical behavior investigation of sewn textile transmission paths on weft-knitted fabrics used for muscle activity monitoring [J]. The Journal of The Textile Institute, 2021, 113(10): 2215-26.
[29] RUPPERT-STROESCU M, BALASUBRAMANIAN M. Effects of stitch classes on the electrical properties of conductive threads [J]. Textile Research Journal, 2017, 88(21): 2454-63.
[30] VIRKKI J, WEI Z, LIU A, et al. Wearable Passive E-Textile UHF RFID Tag Based on a Slotted Patch Antenna with Sewn Ground and Microchip Interconnections [J]. International Journal of Antennas and Propagation, 2017, 2017: 1-8.
[31] ZHANG L, BAIMA M, ANDREW T L. Transforming Commercial Textiles and Threads into Sewable and Weavable Electric Heaters [J]. ACS Appl Mater Interfaces, 2017, 9(37): 32299-307.
[32] SHIN Y-E, LEE J-E, PARK Y, et al. Sewing machine stitching of polyvinylidene fluoride fibers: programmable textile patterns for wearable triboelectric sensors [J]. Journal of Materials Chemistry A, 2018, 6(45): 22879-88.
[33] ALI M, SIDDIQUI M O R, OZDEN YENIGUN E, et al. Evaluation of conductive threads and stitch configurations for heated e-textile applications [J]. Journal of Industrial Textiles, 2025, 55.
[34] KIM H, RHO S, JEONG W. Manufacturing and characterization of conductive threads based on twisting process for applying smartwear [J]. Fashion and Textiles, 2025, 12(1).
[35] WU X, YE S, GAO C, et al. Programmable sewing sensors for preventing neck injuries [J]. Chemical Engineering Journal, 2025, 525.
[36] SAMUEL WESLEY D, RENGASAMY R S. Changes in tensile properties of needle thread in lock stitch sewing [J]. Fibers and Polymers, 2017, 18(2): 390-9.
[37] YANG Y, CHEN Y, LIU Y, et al. Programmable and Scalable Embroidery Textile Resistive Pressure Sensors for Integrated Multifunctional Smart Wearable Systems [J]. Advanced Fiber Materials, 2025, 7(2): 574-86.
[38] XINYU G, WENBO L, FUYI F, et al. Encoded sewing soft textile robots [J]. Science advances, 2024, 10(1): eadk3855-eadk.

© Author(s) 2026. This work is distributed under the Creative Commons BY- 4.0 license:
https://creativecommons.org/licenses/by/4.0/